Astron. Astrophys. 356, 1067–1075 (2000)

ASTRONOMY AND ASTROPHYSICS

The fast and slow Hα chromospheric responses to non-thermal particles produced during the 1991 March 13 hard X-ray/gamma-ray flare at $\sim$ 08 UTC

G. Trottet[1], **E. Rolli**[2], **A. Magun**[3], **C. Barat**[4], **A. Kuznetsov**[5], **R. Sunyaev**[5], **and O. Terekhov**[5]

[1] DASOP, CNRS-UMR 8645, Observatoire de Paris, Section Meudon, 92195 Meudon, France
[2] NUCATE/CRAAE, Unicamp, Rua Rôxo Moreira 1752, 13083-592 Campinas, SP, Brazil
[3] University of Bern, IAP, Sidlerstrasse 5, 3012 Bern, Switzerland
[4] Centre d'Eťude Spatiale des Rayonnements, B.P. 4346, 31029 Toulouse, France
[5] Space Science Institute, Profsoyuznaya 84/32, 117810 Moscow, Russia

Received 27 January 2000 / Accepted 18 February 2000

Abstract. We present a multi-wavelength analysis of the X1.3/-2B solar flare at 8 UTC on 1991 March 13 which includes Hα images obtained by the fast digital Hα-camera at Locarno-Monti at a rate of five images per second, full disk microwave measurements made with a time resolution of 0.1 s by the radiotelescopes in Bern and hard X-ray/gamma-ray data with a $\leq$ 1 s time resolution by PHEBUS on board the GRANAT satellite. This set of multispectral data is used to investigate alternate forms of energy transport from the hot flare corona to the chromosphere. During this large flare, which exhibits two successive episodes of acceleration, energy transport took place within four loop systems of different sizes which expand with time and whose foot points were materialized by four Hα kernels. It is shown that accelerated particles, most probably electrons, are the dominant form of energy transport, so that slower processes, such as conduction fronts, only play little role if any. Such a conlusion is demonstrated by the fact that the time evolution in intensity from the four observed kernels is well reproduced by a linear combination of the hard X-ray count rate and its time integral. Such a relationship, which is first established in this work, indicates that the Hα response to non-thermal electrons consists of two components which evolve on different time scales, typically a few seconds and a few tens of seconds. The amplitude of the slow response is similar for the four kernels during the whole flare. In contrast, the amplitude of the fast response varies from one kernel to the other and is found to be the greater for the larger loop systems during the second and strongest episode of acceleration. Finally, during the first episode of acceleration, the fast Hα response exhibits time variations with typical rise times of $\sim$ 0.4-1.5 s which are nearly coincident with fast hard X-ray pulses of similar rise times. This is, so far, the most convincing evidence for correlated fast time structures in Hα and hard X-rays. The ensemble of these results are discussed in the framework of models which simulate the chromospheric response of a loop atmosphere to heating by non-thermal electrons.

Send offprint requests to: G. Trottet

Key words: Sun: activity – Sun: chromosphere – Sun: flares – Sun: X-rays, gamma rays

1. Introduction

It is widely accepted that a solar flare results from the rapid release of free magnetic energy near the top of active region loops. The dissipation of this energy in the coronal release sites leads to acceleration of electrons and ions to high energies and to direct heating of the plasma and plasma motions. There are basically two forms of energy transport from the primary energy release sites to the regions of energy dissipation in the low-corona and chromosphere, at the footpoints of the flaring loops. The study of the morphology and timing of the Hα line emission with respect to that of the microwave and hard X-ray emission provides a useful test through which one can discriminate between these forms of energy tranport, provided by the different flare models.

The thermal model assumes that most of the energy released goes into the impulsive heating of the plasma near the release site to temperatures above 10^8 K (Brown et al. 1979; Smith & Lillequist 1979; Batchelor et al. 1985). Conduction fronts are formed in the loops and move at the ion sound speed (typically 100-1000 km s^{-1}). The observed microwave and HXR emission arise then predominently from expanding hot sources confined behind the conduction front. Hα starts to rise when the conduction front hits the chromosphere $\sim$ 10 to 20 s after the onset of the microwave and HXR emission for typical loop parameters.

The second scenario, known as the non-thermal thick target model, assumes that most of the energy release goes into the acceleration of particles near the release site (e.g. Brown 1971). Non-thermal electrons which stream down along the magnetic field reach the low corona and upper chromosphere in less than 1 s where they produce the HXR bremsstrahlung emission by thick-target interaction with ambient ions. Below, in the chromosphere, the same electrons are dumped and heat the ambient

medium which leads to an enhanced Hα emission. The rises of the Hα, microwave and HXR emission are thus expected to be simultaneous within less than 1 s. It should be noted that $\lesssim 0.5$ MeV protons can similarily produce enhanced Hα emission (Simnett 1986). Unfortunately, there are no unambiguous radiative signatures of such low energy protons in the solar atmosphere. Observations of linear polarization in the Hα line may, in principle, help to discriminate between electrons and protons (e.g. Vogt & Hénoux 1999), but the time resolution (1 to several minutes) of the few observations made so far is much larger than the typical time scale of energy transport by particles. Canfield & Gayley (1987) have computed the temporal evolution of the Hα line profile using models of Fisher et al. (1985a, 1985b) which simulate the dynamic response of a loop atmosphere to Coulomb heating by a beam of accelerated electrons. They show that the temporal Hα response arises from three distinct physical processes whose relative importance varies over the line profile: a temperature response, an ionization response and a hydrodynamic response. The first two processes are responsible for the fastest time scales, typically < 0.1 s for the temperature response which has its largest amplitude at line center, and ~ 0.5 s for the ionization response which is most apparent in the blue wing. The hydrodynamic response, which is related to the formation of a chromospheric condensation, gives rise to longer time scales (several seconds) and is most apparent in the red wing. Heinzel (1991) who performed similar calculations by using atmosphere models of Karlický (1990) further predicts an anticorrelation between HXR and Hα sub-second pulses.

Studies of the relative timing between Hα and HXR (or microwave observations), all made with ≈ 1 s time resolution, have shown that both forms of energy transport may exist at different sites during the same flare (e.g. Kämpfer & Schöchlin 1982; Kämpfer & Magun 1983; Wülser & Kämpfer 1986). Indeed, at some sites Hα is delayed by 10 s or more with respect to the microwave or HXR while at other sites a synchronism (within 1 to 2 s) is observed between these different emissions. The latter supports the models describing the heating of the chromosphere by non-thermal electrons. A close similarity between the Hα and HXR time profiles was also found in several flares where Hα data with sub-second time resolution were available (Wülser & Marti 1989; de la Beaujardière et al. 1992; Neidig et al. 1993). However, the data were smoothed with integration times above 1 s for noise reduction, so that a study of subsecond Hα structures was not possible.

In this paper we present the comparison of fast (0.2 s) Hα line center imaging observations together with fast microwave (0.1 s) and HXR (0.1–1 s) spectral measurements during the 1991 March 13 flare at 08 UTC. Sects. 2 and 3 present the instruments and the analysis of the observations, respectively. It appears that the time evolution of each of the four Hα kernels observed during this flare can be related in a simple way to the HXR time profile. This finding is discussed in Sect. 4 in the framework of an electron-beam-heated chromosphere. The conclusions are summarized in Sect. 5.

2. Instrumentation

The Hα observations were carried out with a coelostat at the 'Specola Solare Ticinese' in Locarno-Monti, Switzerland. A Zeiss birefringent filter (0.05 nm bandpass) and a fast digital CCD-camera were installed at the focus of the telescope with a focal length of 1.95 m and a free aperture of 0.15 m (Eder 1990). The instrument is an improved version of the one used by Wülser & Marti (1989). Our setup had a field of view (FOV) of $160'' \times 160''$ with a pixel size of $0.92'' \times 0.88''$ and a temporal resolution of 0.2 s. The images were flat-field calibrated and seeing induced shifts were corrected with the help of sunspot positions in the images. The temporal variation of the transparency of the Earth's atmosphere was taken into account by normalizing the image intensity relative to that of a quiet Sun region in the same image.

The microwave observations of the event were made by the patrol radio telescopes in Bern at 3.1, 5.2, 8.4, 11.8, 19.6, 35.0 and 50.0 GHz in right and left circular polarization with a temporal resolution of 0.1 s (e.g. Bruggmann & Magun 1990). The data were calibrated with published absolute quiet-Sun fluxes from Sagamore Hill (see Melnikov & Magun 1998). A sky calibration just ended at 08:01:00 UTC for 3 and 5 GHz and at 08:01:30 UTC for the higher frequencies. Therefore the first few seconds at the onset of the flare are missed at higher frequencies.

The hard X-ray/gamma-ray (HXR/GR) observations were carried out by the PHEBUS experiment on board the GRANAT satellite. PHEBUS has been described in Barat et al. (1988); Barat (1993) and Talon et al. (1993). During the 1991 March 13 flare, HXR/GR data were acquired from 08:01:38 to 08:14:24 UTC. The observations used here consist of spectral measurements performed in the 0.073–89 MeV energy range. Until 08:03:34 UTC spectra have been recorded over 116 energy channels with a variable accumulation time ranging from 0.37 to 0.88 s. After 08:03:34 UTC, 40 channel spectra have been recorded each second below ~ 8 MeV and every 4 seconds above. In addition we have used records of the > 0.073 MeV integral count rate obtained from 08:01:26 to 08:03:06 UTC with a time resolution varying from 8.5 ms to 48 ms, which were integrated to ~ 200 ms, to improve the signal-to-noise ratio.

Finally, we have used a magnetogram recorded at Kitt Peak 16 hours before the flare.

3. Observation

The 1991 March 13 flare around 08 UTC occurred in the NOAA active region 6545 at S10-E44. Fig. 1 displays the temporal evolution of the Hα intensity for two kernels N1 and N2 (see Sect. 3.1 below), of the HXR count rate and of the microwave flux densities. The HXR and microwave time profiles exhibit two impulsive bursts. The first and weaker burst B1 started at $\sim$ 08:01:25 UTC, while the second and more intense one B2, started at $\sim$ 08:03:30 UTC. The Hα emission shows two rises corresponding to those of the HXR count rate and of the microwave emission, but decays on much longer time scales.

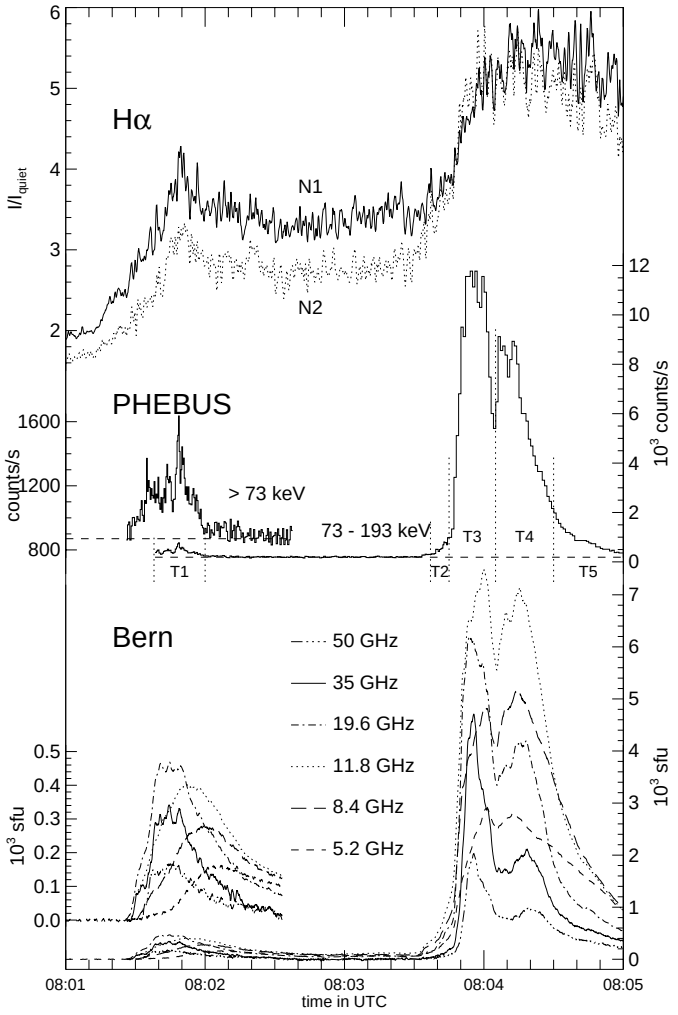

Fig. 1. Temporal evolution of the 1991 March 13 flare. The top curves are the Hα line center intensity in kernels N1 and N2, the middle curves are hard X-ray count rates and the bottom curves are the microwave flux densities. Also shown is an enlargement of the first part of the hard X-ray and microwave flare emission.

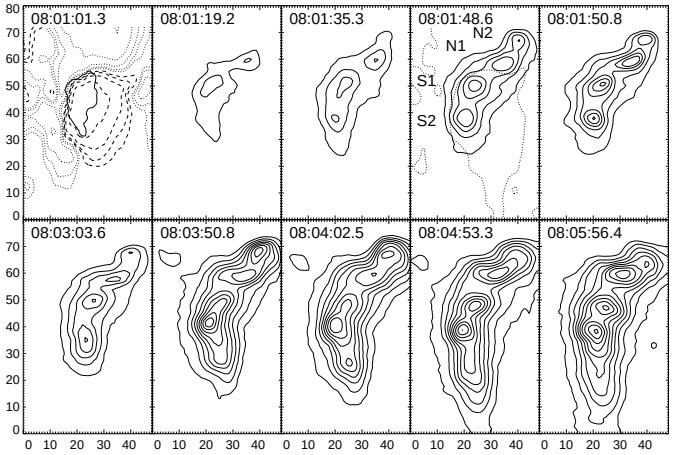

Fig. 2. Time sequence of representative Hα images of the flare. The graduations on both axis are arcseconds. The first frame with the preflare image also shows the Kitt Peak magnetogram from the previous day. Dotted lines represent positive and dashed lines negative magnetic field polarities. The contour levels are 100, 200, 400 and 800 G. The frame at 08:01:48 UTC shows the labeling of the different kernels together with the magnetic neutral line (dotted line). North is at the top, west to the right. The faint emission visible as one contour line NE of the two ribbons in the frames from 08:03:50.8 to 08:04:53.3 is a surge activity not studied in this paper.

3.1. Hα observations

Fig. 2 shows snapshot maps of the Hα emission taken during B1 and B2. The first frame displays the Kitt Peak magnetogram rotated to the time of the Hα observations, and overlaid on the preflare Hα image. During B1 and B2, the bulk of the Hα emission arises from two ribbons, located on each side of a magnetic neutral line (dotted line in the frame at 08:01:48.6 UTC). Bright kernels are visible within the two ribbons. They are labelled N1 and N2 for the northern ribbon and S1, S2 for the southern ribbon which respectively overlay positive and negative magnetic polarities. As the flare evolves the two ribbons expand further away from the magnetic neutral line. Hα full Sun patrol observations obtained every minute by the 3 λ Hα heliograph at Paris-Meudon observatory (courtesy of Z. Mouradian) indicate that until 08:05 UTC the Hα flaring emission is entirely contained in the FOV of the fast Hα camera. After 08:05 UTC, i.e. at the end of B2, the northern ribbon extends south-westward from N2, outside the FOV of the fast camera. The intensity $I/I_{\rm quiet}$ of each of the four kernels has been computed as a function of time by averaging over a square of 4.8 arcsec^2 (6 pixels). A change of the averaging area by a factor of 2 only influences the amplitude but not the shape of the temporal evolution. The time evolution of the Hα intensity, shown for N1 and N2 in Fig. 1, is globally similar for the four kernels. In particular, the emission of each of the four kernels shows rapid rises corresponding to those of B1 and B2.

3.2. HXR/GR and microwave observations

Spectral analysis of the PHEBUS data has been performed for count spectra accumulated over the four intervals of time (T1 to T4) marked by vertical dashed line on the >73 keV time profile shown in Fig. 1. During T1 and T2, which correspond to B1 and the initial slow rise of B2, no significant emission is detected for photon energies ($h\nu$) above ~ 0.2 MeV. The photon spectrum was fitted to a single power law given by $A(h\nu/0.1)^{-\gamma_1}$, where $h\nu$ is in MeV, A (photons cm^{-2} MeV^{-1} s^{-1}) is the photon flux at 0.1 MeV and γ_1 the power law index. During T3 and T4, GR emission is detected up to ~ 8 to 10 MeV, and marginally significant 2.23 MeV and prompt gamma-ray line emissions are present. This time period (T3 and T4) starts with the rapid rise of the >73 keV emission which follows the initial slow rise of B2 and covers the two main peaks of B2 till the slow decay of the HXR/GR and microwave emissions. For these two peaks, the photon spectrum of the continuum is well represented by a broken power law. The corresponding parameters are then A and γ_1 as before, $E_{\rm break}$ the break energy and γ_2 the power law index

Table 1. Photon spectrum parameters and estimated electron fluxes during T1, T2, T3 and T4.

time interval	$A(0.1MeV)$ (ph/MeV cm^2 s)	$E_{\rm break}$ (MeV)	γ_1	γ_2	P_{100} (erg s^{-1})	P_{20} (erg s^{-1})
T1: 08:01:38–08:02:00	35	–	5.6 ± 0.1	–	$1.9\ 10^{26}$	$3.0\ 10^{29}$
T2: 08:03:37–08:03:45	50	–	5.7 ± 0.1	–	$2.8\ 10^{26}$	$5.4\ 10^{29}$
T3: 08:03:45–08:04:05	4480	0.39 ± 0.05	5.0 ± 0.1	3.1 ± 0.3	$2.0\ 10^{28}$	$1.3\ 10^{31}$
T4: 08:04:05–08:04:30	3040	0.35 ± 0.05	5.0 ± 0.1	2.7 ± 0.2	$1.4\ 10^{28}$	$8.6\ 10^{30}$

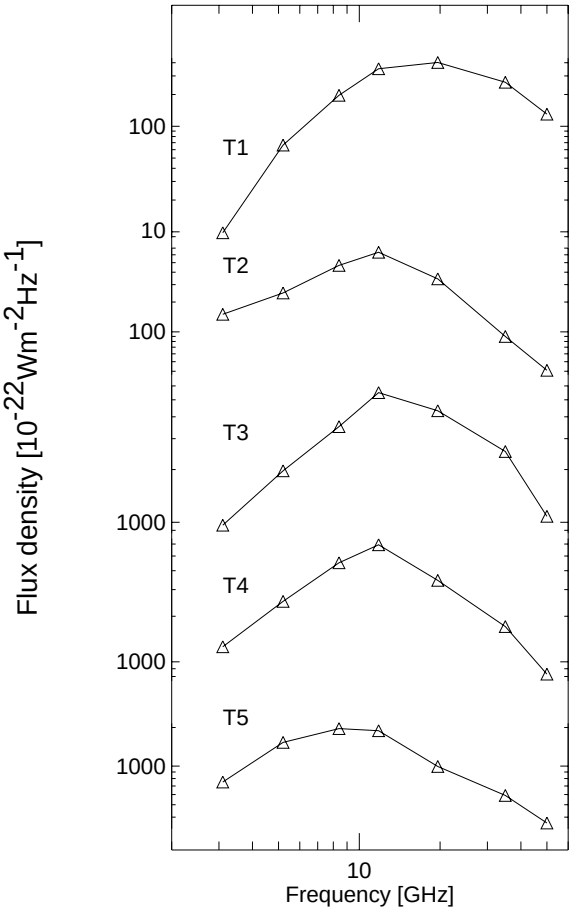

Fig. 3. The microwave spectrum for the five intervals of time (T1–T5) during the 1991 March 13 flare. T1 is during the first part of the HXR/GR event (burst B1) and T2 to T5 cover the second part (burst B2).

for h$\nu > \mathrm{E_{break}}$. The values of A, $\mathrm{E_{break}}$, γ_1 and γ_2 are given in Table 1 for the four intervals of time under consideration. Table 1 also shows the power $\mathrm{P_{100}}$ (resp. $\mathrm{P_{20}}$) deposited in the chromosphere by > 100 keV (resp. > 20 keV) HXR producing electrons. $\mathrm{P_{100}}$ has been estimated by assuming that the bulk of the HXR emission is the result of thick target bremsstrahlung of > 100 keV electrons and by using the low energy part of the photon spectrum and thick target calculations by Hudson, Canfield & Kane (1978). $\mathrm{P_{20}}$ has been obtained by extrapolating the > 73 keV HXR photon spectrum down to 20 keV.

Fig. 3 displays the microwave spectrum during the five intervals of time labelled T1, T2, T3, T4 and T5 (Fig. 1). A detailed discussion of the time evolution of the microwave spectrum, which is beyond the scope of this paper, has been given in Melnikov & Magun (1998) for the second burst B2. Fig. 3 shows that the radio emission at 35 and 50 GHz remains optically thin during the whole flare. Taking the shape of the optically thin part of the microwave spectrum as ν^α (where ν is the radio frequency) we determined α from the ratio of the flux densities measured at 35 and 50 GHz. The spectral index $\delta_{\rm R}$ of the microwave producing electrons is approximatly given by $\delta_{\rm R} \approx (1.22 - \alpha)/0.9$ (Dulk & Marsh 1982). For thick target interactions the spectal index $\delta_{\rm X}$ of the HXR/GR producing electrons is given by $\delta_{\rm X} = \gamma + 1$ where γ is the slope of the HXR/GR photon spectrum (e.g. Brown 1971). As a first approximation we take $\delta_{\rm X1} = \gamma_1 + 1$ below $\mathrm{E_{break}}$ and $\delta_{\rm X2} = \gamma_2 + 1$ above (see Trottet et al. 1998).The values of α, $\delta_{\rm R}$, $\delta_{\rm X1}$ and $\delta_{\rm X2}$ obtained during T1, T2, T3 and T4 are given in Table 2 which also provides the turnover frequency $\nu_{\rm max}$ of the corresponding microwave spectrum. The comparison of $\delta_{\rm R}$ with $\delta_{\rm X1,2}$ indicates that:

Table 2. Microwave spectrum parameters and indices of the electron spectrum deduced from microwave and HXR/GR observations during T1, T2, T3 and T4.

time interval	$\nu_{\rm max}$ (GHz)	α	$\delta_{\rm R}$	$\delta_{\rm X1}$	$\delta_{\rm X2}$
T1: 08:01:38–08:02:00	$\sim$20	-1.9	3.5 ± 0.3	6.6 ± 0.2	
T2: 08:03:37–08:03:45	$\sim$12	-2.2	3.8 ± 0.3	6.7 ± 0.2	
T3: 08:03:45–08:04:05	$\sim$12	-2.4	4.0 ± 0.2	6.0 ± 0.3	4.1 ± 0.3
T4: 08:04:05–08:04:30	$\sim$12	-2.0	3.6 ± 0.2	6.0 ± 0.3	3.7 ± 0.2

- During T3 and T4 (i.e. during the two peaks of B2), where γ_2 could be estimated, $\delta_{\rm R} \approx \delta_{\rm X2}$. This indicates that the microwave emission is produced by the high energy part of the HXR/GR emitting electrons.
- During T1 and T2 (i.e. during B1 and the initial slow rise of B2) the values of $\delta_{\rm R}$ are comparable to those obtained during T3 and T4. This strongly suggests that high energy electrons, emitting the upper part of the spectrum ($\sim \delta_{\rm X2}$), have been produced since the very beginning of B1, their flux being too small to give a detectable HXR/GR emission above ~ 200 keV.

These characteristics are similar to those found in other large HXR/GR flares (e.g. Trottet et al. 1998 and references therein). Similar results have also been deduced from the comparison of the HXR and radio millimeter emissions during smaller flares

for which the sensitivity of HXR/GR detectors is not sufficient to measure the high energy part ($h\nu > E_{\rm break}$) of the HXR/GR emission (e.g. Kundu et al. 1994; Silva et al. 1997; Raulin et al. 1999).

Fig. 3 shows that the shape of the microwave spectrum of B1 and B2 is indicative for an inhomogeneous radio source region that, for example, consists of magnetic field loops of different sizes. Indeed: (i) except during T1 the spectral rise is flater than $\nu^{2.5}$ (resp. $\nu^{2.9}$) as would be expected for an emission from relativistic (resp. midly-relativistic) electrons in a uniform magnetic field (e.g.Dulk & Marsh 1982); (ii) during T1, as well as during T3 and T5, the spectrum is rather flat around the turnover frequency $\nu_{\rm max}$ which, again, is a signature of an inhomogeneous source (e.g. Klein & Trottet 1984). The turnover frequency at $\sim$ 20 GHz during B1 (T1) is shifted towards lower frequencies ($\sim$ 12 GHz) during B2 (T2, T3, T4). Such a shift of $\nu_{\rm max}$ requires that self absorption, Razin suppression or free-free absorption in the ambient plasma, become less effective at lower frequencies during B2. Thus, the shift of $\nu_{\rm max}$ to lower frequencies reflects most likely a decrease of the magnetic field, of the ambient density and of the density of emitting electrons along the line of sight or a combination of the three. In any case this indicates that most of the microwave emission detected during B2 arises from more extended sources than during B1. It should be noted that during the late decay of B2 (T5) $\nu_{\rm max}$ drifts towards even lower frequencies ($\sim$ 8 GHz) and that the spectrum of microwave emitting electrons hardens ($\delta_{\rm R} \sim 2.9$). This has been discussed by Melnikov & Magun (1998) in the framework of coronal trapping of the emitting electrons. During T5, the HXR/GR rates are too low to enable us to determine γ_2. However, γ_1 is found to decrease with time which is also an indication for trapping of the hard X-ray emitting electrons with lower energies than those responsible for the optically thin microwave emission.

In summary, the above comparison between the HXR/GR and microwave emissions provides evidence indicating that:

- The microwave emission at 35 and 50 GHz is produced during the whole event (i.e. during B1 and B2) by a population of high energy electrons with the same spectrum as that producing the HXR/GR radiation above $E_{\rm break} \sim 350$ keV.
- The microwave emission arises from a complex region which consists of magnetic loops with various sizes. During B2 the microwave emission is predominantly radiated by loops of larger sizes than during B1. This is consistent with the Hα observations which show that the distances between kernels in opposite field polarities increase from B1 to B2 and even during B2 (see Fig. 2).

3.3. Comparison between Hα and HXR/GR observations

As stated in Sect. 3.1 the four Hα kernels exhibit a similar time evolution. During both B1 and B2 the Hα time profile of each kernel exhibits a fast component that is superposed on a slowly varying component. The fast component shows two rises corresponding to those of the $>$ 73 keV HXR count rate. This led us to assume that at each time t in a given interval of time from t1 to t2, and for each kernel i, the time history of the relative Hα intensity $\Delta {\rm I_i(t)}$ is related to the HXR time evolution by:

$$\Delta {\rm I_i(t)} = \frac{{\rm I_i(t) - I_i^{back}}}{\rm I_{quiet}} = {\rm A_i}\frac{\rm C_X(t)}{\rm C_X^{max}} + {\rm B_i}\frac{\int_{\rm t1}^{\rm t} {\rm C_X(t')dt'}}{\int_{\rm t1}^{\rm t2} {\rm C_X(t')dt'}} \quad (1)$$

where ${\rm I_i(t)/I_{quiet}}$ is the relative Hα intensity of kernel i, ${\rm I_i^{back}/I_{quiet}}$ its relative level before the burst (B1 or B2), $\rm A_i$ and $\rm B_i$ are constants, $\rm C_X(t)$ the instantaneous $>$ 73 keV HXR count rate and $\rm C_X^{max}$ its maximum value between t1 and t2. The indices i=1, 2, 3, 4 mark the kernels N2, N1, S1 and S2 respectively.

The above relation assumes that:

- the fast Hα component is proportional to the $>$ 73 keV HXR count rate which is practically proportional to the power $\rm P_{100}$ (resp.$\rm P_{20}$) deposited into the chromosphere by the HXR/GR emitting electrons;
- the slow Hα component is proportional to the integral of the HXR count rate between t1 and t which is roughly proportional to the energy deposited into the chromosphere by the non-thermal electrons between t1 and t.

Eq. 1 has been applied separately for B1 and B2. The free parameters $\rm A_i$ and $\rm B_i$ have been determined for each kernel by using a χ^2 minimization algorithm.

The interval of time considered for B1 is T1. Fig. 4 (left) shows that, during B1, the observed Hα time profile (thin line) of each of the four kernels is nicely reproduced by that modelled (thick line) with the simple two parameter model defined by Eq. 1 ($\chi^2 \sim 0.4-0.7$). The dashed lines show the slowly varying component modelled for each kernel.

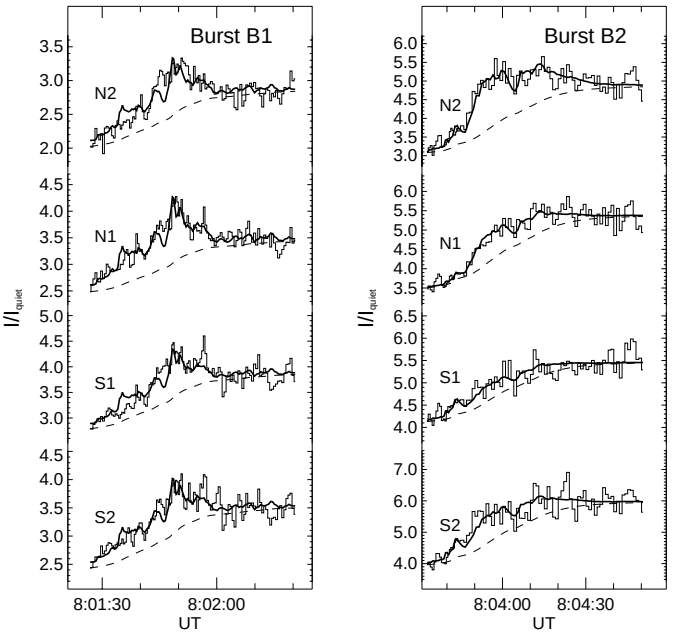

Fig. 4. Observed (thin line) and modelled (thick line) time evolution of the Hα intensity of the four kernels (N2, N1, S1 and S2) during B1 (left) and during B2 (right). In both panels the dashed lines show the modelled slowly varying component for each kernel.

During B2 we have considered two successive injections of HXR emitting electrons, taken as C_X(t) over T2 and over T3 to T5 respectively. The first injection corresponds to the initial slow rise of B2 whereas the second one, which starts with the rapid HXR and GR rise, covers the most energetic part of B2. However, only a single slowly varying term has been computed, as due to the low HXR count rate during T2, relative to that during T3 and T4, the splitting of the slowly varying component into two parts would not significantly affect the results. For each kernel the free parameters are then: A_i^1, A_i^2 for the fast components during T2 and T3, T4 and T5 respectively and B_i for the slow component during the whole B2 burst. The results obtained for B2 are shown in Fig. 4 (right). Here again, there is a good agreement ($\chi^2 \sim$ 0.5–0.9) between observed and computed time profiles. It should be noticed that χ^2 ($\sim$ 2.5) increases significantly when only one single electron injection over the time period, consisting of T2, T3, T4 and T5, is taken into acount.

4. Discussion

The 1991 March 13 HXR/GR impulsive flare at $\sim$ 08:00 UTC exhibits two successive HXR and microwave bursts referred to as B1 and B2 in Sect. 3. During the whole event, the Hα emission arises from four kernels (N1, N2, S1 and S2 in Fig. 2). Although the power deposited in the chromosphere by the HXR producing electrons is about thirty times larger during B2 than during B1 (see Table 1), the relationship between the temporal evolutions of the fast Hα emission and the HXR count rate is found to be the same for each Hα kernel during both B1 and B2. The intensity time profile of a given Hα kernel is indeed well represented by a linear combination of two components which evolves on different time scales, i.e. the HXR count rate which varies on $\leq$ 1 s to $\sim$ 10 s time scales and its time integral which smoothly increases with time. This analysis only concerns the Hα emission observed during both B1 and B2 which appear as two separated HXR bursts above 73 keV. However, observations made by the *ULYSSES*/GRB instrument indicate that the $\sim$ 25 keV HXR emission shows a plateau between B1 and B2, like Hα, and a gradual burst which lasts for $\sim$ 7 to 8 minutes after the end of B2 (K. Hurley, private communication). This suggests that the Hα emission may be also related to the HXR emission between B1 and B2 and after B2. Further analysis is needed to investigate if such a relationship is similar to that described by Eq. 1.

The excellent agreement of the observed Hα intensity time profile with that modelled with Eq. 1 strongly suggests that Hα results from energy transport by non-thermal electrons during both B1 and B2. The measurements of tangential linear polarization of the Hα line during the impulsive part of some HXR bursts support this conclusion (Vogt & Hénoux 1999). However, Vogt & Hénoux (1999) pointed out that low energy protons mirroring in a converging magnetic field could also produce the observed polarization. If this would be the case, our results would imply a close synchronism ($<$ 1 s) between the acceleration of $<$ 500 keV protons and $>$ 73 keV electrons.

A quantitative interpretation of the present results would need: (i) soft X-ray imaging observations which provide constraints on the model atmosphere of the different loop systems, such as the time evolution of temperature and emission measure; (ii) hard X-ray imaging observations in order to estimate which fraction of the accelerated electrons is injected towards each kernel and (iii) measurements of the Hα line profile in order to identify the different physical processes which contribute to the formation of Hα at different chromospheric depths. In the following we thus consider that Hα is produced by non-thermal electrons and we qualitatively discuss our findings in the framework of the conventional non-thermal thick-target model which has successfully explained various radiative signatures of non-thermal electrons including HXR, microwaves and Hα (e.g. Canfield & Gayley 1987; Pick et al.1990; Miller et al 1997 and references therein)

4.1. Magnetic field structure

In the non-thermal thick-target model, electrons are accelerated in the corona near the top of loops with sizes ranging typically from a few 10^3 km to a few 10^4 km. The HXR thick-target emission and the Hα kernels are produced at the feet of the loops into which electrons stream from the coronal acceleration region to the chromosphere. Thus, the Hα kernels, whose time histories are correlated to the HXR time profile, materialize the feet of loop systems connected to the acceleration region. During the flare under study, the existence of four kernels overlying opposite polarities of the photospheric magnetic field suggests that four loop systems are involved: LS11, LS12, LS21 and LS22 which connect N1 to S1, N1 to S2, N2 to S1 and N2 to S2 respectively. Taking the distance between kernels overlying fields of opposite polarities as typical sizes of the different loop systems we obtain approximately 10^4 km, 1.7 10^4 km and 2.5 10^4 km for LS11, LS12 and LS21 and LS22 respectively. The magnetic structure into which electrons are accelerated and in which they interact to produce the observed HXR, microwave and Hα emission appears thus to be complex as each kernel is associated to two loop systems. Such a complexity is also revealed by the shape of the microwave spectrum as emphasized in Sect. 3.2. Moreover, it should be remarked that the increase of the number of accelerated electrons from B1 to B2 is associated with an expansion of the different loop systems (Sect. 3.2). This suggests that an increase of the flaring loop size is associated with an increase of the number of accelerated electrons.

4.2. The slow Hα response

For each of the four kernels, the slow Hα response is found to be proportional to the time integral of the HXR count rate that is, to the time integral of the power deposited by the non-thermal electrons in the associated thick-target HXR emitting source. The values of the coefficients of proportionality, $b_i = B_i/\Sigma B_i$, are given in Tables 3 and 4 for B1 and B2 respectively. Such a contribution to the Hα time profile has not yet been explicitly incorporated in models (e.g. Canfield & Gay-

Table 3. The cefficients $a_i = A_i/\Sigma A_i$ and $b_i = B_i/\Sigma B_i$ obtained from the application of Eq. 1 to the Hα observations during B1

Kernel	N2	N1	S1	S2
a	0.21	0.31	0.24	0.24
b	0.21	0.25	0.27	0.27

Table 4. Same as Table 3 for B2

Kernel	N2	N1	S1	S2
a (1^{rst} inj.)	0.32	0.10	0.22	0.36
a (2^{nd} inj.)	0.41	0.22	0.10	0.27
b	0.26	0.27	0.19	0.28

ley 1987; Heinzel & Karlický 1992) which simulate the Hα response to non-thermal electron beams. For most impulsive HXR bursts, it has been shown that the time history of the time integrated HXR count rate closely matches the rising portion of the soft X-ray emission (the so-called Neupert Effect) i.e. of the thermal bremsstrahlung from the hot loop plasma (e.g. Neupert 1968; Dennis & Zarro 1990). The cause of this behavior has been interpreted in various ways which all include heating of the loop plasma by the accelerated electrons (e.g. Brown 1971; Syrovatskii & Shmeleva 1972) or by accelerated electrons and and some other agent such as electric fields which simultaneously accelerate the electrons (e.g. Holman et al.1989) or turbulence (e.g. Lee et al. 1995). Processes leading to density enhancements of the loop plasma such as chromospheric evaporation may also play a role (e.g. Li et al. 1993). This indicates that, for the studied event, the slow Hα response to non-thermal electrons is partly due to some continuous heat flux from the corona to the chromosphere as was suggested by Gräter (1990) for other flares. Although the Hα kernels are at the feet of loop systems of different sizes and the energy content in electrons is much higher during B2 than during B1, the coefficients b_i do not vary much from one kernel to the other and from B1 to B2. Such a result is quite surprising because the slow Hα response of a given kernel is expected to depend both upon which fraction of the non-thermal electrons has been injected in each loop system, and upon the dynamical response of the atmosphere which is probably different from one loop system to the other.

4.3. The fast Hα response

The fast Hα response of a given kernel is found to be proportional to the time profile of the HXR count rate that is, to the time evolution of the power supplied by the accelerated electrons to the thick-target HXR emitting source associated with this kernel. The values of the coefficient of proportionality $a_i = A_i/\Sigma A_i$ are given in Tables 3 and 4 for B1 and B2 respectively. During B1 the coefficients a_i are about the same for the four Hα kernels, the response of N1 being slightly, but significantly, stronger than that of the other kernels (see Table 3). The situation is quite different during B2. For both injections of electrons the strongest responses are obtained for N2 and S2 while the response of S1 during the first injection and that of N1 during the second one are weak (see Table 4). Because N1 (resp. S1) are common feet of LS11 and LS12 (resp. LS11 and LS21) it is suggestive that the fast response of the smallest loop system (LS11) is the weakest. Here again, the available data do not allow us to estimate which fraction of the energy transported by the electrons is deposited in each kernel because the model atmosphere associated to that kernel is unknown. The simplest, very crude, assumption is to consider that the atmosphere model is nearly the same for all kernels. Our results would then indicate that:

- during B1 the four kernels receive about the same flux of non-thermal energy. Taking 20 arcsec^2 for the typical kernel area (see Fig. 2) and the value of P_{20} given in Table 1 the energy flux deposited by > 20 keV electrons in each kernel is $\sim$ 7 x 10^{11} ergs cm^{-2} s^{-1}.
- during B2 the energy is predominently transported along the larger loop systems and the energy flux deposited by $>$ 20 keV electrons in N2 or S2 is $\sim$ 1 x 10^{12} ergs cm^{-2} s^{-1} and $\sim$ 2-3 x 10^{13} ergs cm^{-2} s^{-1} for the first and second injections respectively.

This latter statement is supported by the fact that during B2 the microwave emission arises predominently from the larger loop systems (see Sect. 3.2). We thus conclude that the differences in the fast Hα responses of the four kernels from B1 to B2 are due, at least partly, to changes of the relative numbers of electrons which propagate in the different loop systems. It should be noted that energy transport takes place preferentially in the larger loop systems with a larger number of accelerated electrons.

The close similarity between the time profiles of the HXR count rate and of the fast Hα response of each kernel is qualitatively in agreement with the results of models by e.g. Canfield & Gayley (1987) and Heinzel & Karlický (1992). Indeed, these models indicate that Hα should be an excellent tracer for the time evolution of the power deposited by accelerated electrons in the chromosphere, that is of the HXR rate for thick-target interactions. Moreover, the initial response to intense beam variations is generally expected to be more rapid than the electron transit time from the acceleration region, so that the shortest time scales of Hα variations are governed by the shortest time scales of the HXR emission. For the Hα line center, these short time scales should be associated to the rises of fast HXR variations (Canfield & Gayley 1987). For the present flare, the shortest variations of the HXR rate can only be studied during B1 where the HXR measurements were obtained with a < 1 s time resolution ($\sim$ 200 ms). As an example Fig. 5 displays the time profiles of the fast Hα emission of N1 (largest a_i) and of the > 73 keV HXR count rate during B1. The Hα emission tracks the HXR count rate, the coefficient of cross-correlation being $\sim$ 0.84 for a 0 ± 0.5 s lag. The HXR emission exhibits significant pulses with rise times ranging from $\sim$ 0.4 s to $\sim$ 1.5 s as it is generally observed for most impulsive bursts (e.g. Aschwanden et al. 1995; Vilmer et al. 1996). The Hα emission also shows time structures with similar rise times. Although some of these fast Hα variations are probably due to remaining seeing effects. there is a clear correspondence between HXR and Hα pulses.

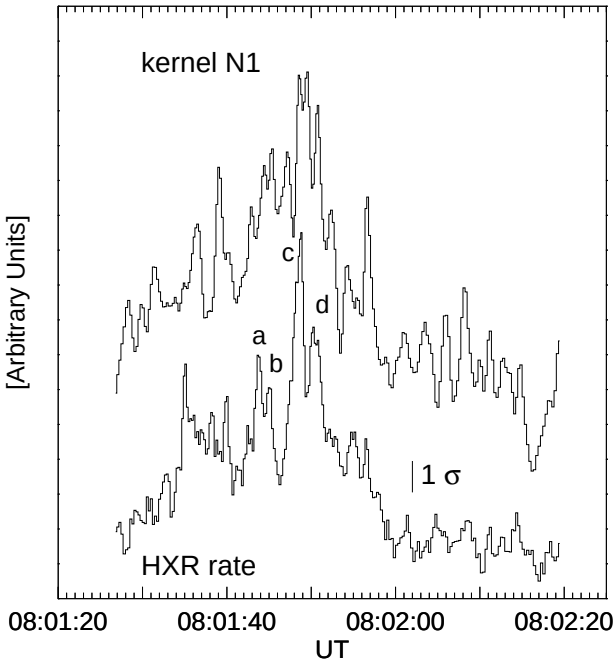

Fig. 5. Time evolution of the fast Hα intensity response of kern el N1 and of the $>$ 73 keV HXR rate during B1. HXR peaks marked a, b, c and d have corresponding ones in Hα (see text).

In particular, HXR pulses marked a, b, c and d on Fig. 5, correspond to fast rises of the Hα emission. This is also the case for the other kernels (see Fig. 4 left panel) except may be for N2 (lowest a_i). Fig. 5 also shows that Hα seems sometimes to rise 300 to 500 ms later than the HXR emission. Such a small delay, which is not expected from the models, may not be real and may just reflect that the time profiles of both emissions exhibit successive pulses which partially overlap. Because the Hα response to a HXR pulse (single electron beam) is generally expected to last longer than the HXR pulse (see Fig. 2 in Canfield & Gayley 1987), the observed onset of a fast Hα rise will be occasionally detected after that of the corresponding HXR rise. So far, models generally consider a single magnetic loop and a single electron beam which turns on instantaneously and whose energy flux ($\leq 10^{12}$ ergs cm^{-2} s^{-1}) is much smaller than those involved in the present event, with the computed Hα emission strongly depending on the parameters describing both the loop and the beam. Thus the expectations from these models should not be compared in details to the present findings which have been obtained for a flare where several loop systems are involved and where the electron injection function shows a complex time evolution. Nevertheless our results, in particular the correspondence between HXR and Hα pulses with $\lesssim 1$ s rise times, basically agree with the essential features of the models.

5. Conclusions

In this paper we have performed a detailed comparison of Hα line center imaging observations with microwave and HXR/GR spectral measurements, obtained with ≤ 1 s time resolution during a large X1.3/2B flare. This data have been used to infer the magnetic field structure which connects the hot flare corona to the chromosphere and to discriminate between alternate forms of energy transport within this structure. For the flare under study, the main results of our analysis can be summarized as follows:

- Energy transport takes place in four loop systems with sizes ranging from approximately 10^4 to 2.5 10^4 km. These loop systems are not static but expand in the course of the flare as the two flare ribbons move apart from each other.
- The four Hα kernels, which materialize the foot points of the four loop systems, show a similar time evolution. During the two successive impulsive microwave and ($>$ 73 keV) HXR bursts (referred to as B1 and B2 in Sect. 3), this time evolution is well fitted by a linear combination of the time profile of the HXR count rate and its time integral (see Eq. 1). Such a close relationship between the Hα and the HXR emission strongly suggest that non-thermal electrons are the dominant energy transport process within the different loop systems during both B1 and B2. An alternative energy transport may be possible by low energy ($<$ 500 keV) protons provided that they are accelerated in close synchronism with $>$ 20 keV electrons. In any case, our results indicate that slower transport processes, such as by conduction fronts, which have been found to be effective at some sites in less energetic flares (see Sect. 1), do not seem to play a major role, if any, in this large GR flare. This suggests that during large GR flares most of the primary energy release goes into particle acceleration while in less energetic flares the relative amounts of energy which go into direct heating and acceleration may vary from one loop system to the other (e.g. Benz et al. 1994 and references therein).
- According to Eq. 1 the temporal response of a given Hα kernel to accelerated particles consists of a fast and a slowly varying component. The latter, which evolves like the time integral of the HXR count rate, i.e. like the soft X-ray emission of the loop systems associated to that kernel, shows approximately the same amplitude for the four kernels during both B1 and B2. Although the present data set did not allow us to fully understand the physical origin of this slow response (continuous heat flux from the hot corona or chromospheric evaporation) its intensity appears, surprisingly, to depend only weakly on the loop model parameters which are probably different from one loop system to the other. In contrast, the fast Hα response, which matches the HXR count rate, is similar for the four kernels during B1, but varies from one kernel to the other during B2 where the largest responses are found for the largest loop systems. This indicates that the energy transport is predominant in the largest loops, i.e. when the number of accelerated particles is largest. Furthermore during B2, our results suggest that the relative amounts of accelerated particles injected into the four loop systems vary from the first to the second injection, i.e. when the number of accelerated electrons starts to increase dramatically (see Sect. 4.3). This is consistent whith former multi-wavelength analysis of GR flares which

indicate that changes in the characteristics of the accelerated particles are associated to changes of the magnetic pattern traced by these particles (e.g. Chupp et al 1993; Trottet et al. 1994; Trottet et al. 1998).

- The present data provide for the first time evidence for nearly simultaneous Hα and HXR pulses with typical rise times in the range of $\sim$ 0.4 to 1.5 s. This is broadly consistent with the essential features of models simulating the Hα response to non-thermal electrons which heat a loop atmosphere (e.g. Canfield & Gayley 1987; Heinzel 1991). However, it is premature to compare our results with these models which apply to a much more simple field geometry, idealized electron injection functions and to much less energetic electron populations than those involved in the present flare.

Acknowledgements. We are grateful to J.-C. Hénoux for his illuminating suggestions and to G. Chambe and K.-L. Klein for critical discussions. We would like to thank the 'Associazione Specola Solare Ticinese', Switzerland, for its hospitality during the observations. This present work was supported by FAPESP under grants No. 97/00243-6 and 93/03321-7, by the Swiss National Science Foundation under grant No. 20-42265.94 and by the French-Bresilian program of exchange of scientists (CNRS-CNPq contract 4130).

References

Aschwanden M.J., Schwartz R.A., Alt D.M., 1995, ApJ 447, 923
Batchelor D.A., Crannell C.J., Wiehl H.J., Magun A., 1985, ApJ 295, 258
Barat C., Cotin F., Niel M., et al., 1988, In: Share G.H., Gehrels N. (eds.) Nuclear Spectroscopy of Astrophysical Sources. AIP Conf. Proc. 170, p. 395
Barat C., 1993, A&AS 97, 43
Benz A.O., Kosugi T., Aschwanden M.J., et al., 1994, Solar Phys. 153, 33
de la Beaujardière J.-F., Kiplinger A.L., Canfield R.C., 1992, ApJ 401, 761
Brown J.C., 1971, Solar Phys. 18, 489
Brown J.C., Smith D.F., Spicer D.S., 1979, ApJ 228, 592
Bruggmann G., Magun A., 1990, A&A 239, 347
Canfield R.C., Gayley K.G., 1987, ApJ 322, 999
Chupp E.L., Trottet G., Marschhäuser H., et al., 1993, A&A 275, 602
Dennis B.R., Zarro D.M., 1992, Solar Phys. 146, 177
Dulk G.A., Marsh K.A., 1982, ApJ 259, 350
Eder S., 1990, Diploma Thesis, Institute of Applied Physics, University of Bern, Switzerland
Fisher G.H., Canfield R.C., McClymont A.N., 1985a, ApJ 289, 425
Fisher G.H., Canfield R.C., McClymont A.N., 1985b, ApJ 289, 434
Gräter M., 1990, Solar Phys. 130, 337
Heinzel P., 1991, Solar Phys. 135, 65
Heinzel P., Karlický M., 1992, In: Svestka Z., Jackson B.V., Machado M.E. (eds.) Eruptive Solar Flares. IAU colloquium No. 133, p. 359
Holman G.D., Kundu M.R., Kane S.R., 1989, ApJ 345, 1050
Hudson H.S., Canfield R.C., Kane S.R., 1978, Solar Phys. 60, 137
Kämpfer N., Magun A., 1983, ApJ 274, 910
Kämpfer N., Schöchlin W., 1982, Solar Phys. 78, 215
Karlický M., 1990, Solar Phys. 130, 347
Klein K.-L., Trottet G., 1984, A&A 141, 67
Kundu M.R., White S.M., Gopalswamy N., Lim J., 1994, ApJS 90, 599
Lee T.T., Petrosian V., McTiernan J.M., 1995, ApJ 448, 915
Li P., Emslie A.G., Mariska J.T., 1993, ApJ 417, 313
Melnikov V.F., Magun A., 1998, Solar Phys. 178, 153
Miller J.A., Cargill P.J., Emslie G.A., et al., 1997, JGR 102, 14631
Neidig D.F., Kiplinger A.L., Cohl H.S., Wiborg P.H., 1993, ApJ 406, 306
Neupert W.M., 1968, ApJ 153, L59
Pick M., Klein K.-L., Trottet G., 1990, ApJS 73, 165
Raulin J.-P., White S.M., Kundu M.R., Silva A.V.R., Shibasaki K., 1999, ApJ 522, 547
Silva A.V.R., Gary D.E., White S.M., Lin R.P., De Pater I., 1997 Solar Phys. 175, 157
Simnett G.M., 1986, Solar Phys. 99, 291
Smith D.F., Lillequist C.G., 1979, ApJ 232, 582
Syrovatskii S.I., Shmeleva O.P., 1972, SvA-AJ 16, 273
Talon R., Trottet G., Vilmer N., et al., 1993, Solar Phys. 147, 137
Trottet G., Chupp E.L., Marschhäuser H., et al., 1994, A&A 288, 647
Trottet G., Vilmer N., Barat C., et al., 1998, A&A 334, 1099
Vilmer N., Trottet G., Verhagen H., et al., 1996 In: Ramaty R., Mandzhavidze N., Hua X.-M. (eds.) High Energy Solar Physics. AIP Conf. Proc. 374, p. 311
Vogt E., Hénoux J.-C., 1999, A&A 349,283
Wülser J.-P., Marti H., 1989, ApJ 341, 1088
Wülser J.-P. Kämpfer N., 1986, In: Dennis B.R., Orwing L.E., Kiplinger A.L. (eds.) Rapid Fluctuations in Solar Flares. NASA CP-2449, p. 301